Lithium stabilization of amorphous ZrO2

Stephens, Gareth Frank; Wilson, Jack; Curling, Simon; He, Guanze; Thomas, P. John; Williams, David; Ortner, Susan; Grovenor, Chris; Rushton, Michael; Cole-Baker, Aidan; Middleburgh, Simon

Progress in Nuclear Energy

DOI:
10.1016/j.pnucene.2024.105165

E-pub ahead of print: 06/05/2024

Publisher's PDF, also known as Version of record

Progress in Nuclear Energy 171 (2024) 105165

Contents lists available at ScienceDirect

Progress in Nuclear Energy

journal homepage: www.elsevier.com/locate/pnucene

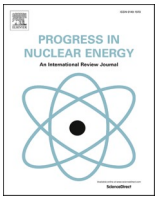

Lithium stabilization of amorphous ZrO_2

Gareth F. Stephens [a,*], Jack A. Wilson [a], Simon F. Curling [b], Guanze He [c], P. John Thomas [a], David W. Williams [a], Susan Ortner [d], Chris Grovenor [c], Michael J.D. Rushton [a], Aidan Cole- Baker [a], Simon C. Middleburgh [a]

[a] Nuclear Futures Institute, Bangor University, Bangor, LL57 1UT, UK
[b] BioComposites Centre, Bangor University, Deiniol Road, Bangor LL57 2UW, UK
[c] Department of Materials, University of Oxford, Parks Road, OX1 3PH Oxford, UK
[d] National Nuclear Laboratory, Culham Science Centre, Abingdon, Oxfordshire OX14 3DB, UK

A B S T R A C T

Small modular reactors (SMRs) are a key option to aid the worldwide net zero targets for carbon emissions. Some pressurised water reactors aim to operate with a boron-free coolant chemistry for simplification in plant design. In the absence of boron, Li has been found to accelerate the corrosion of the zirconium-based alloy fuel cladding under certain conditions and concentrations within pressurised water reactors (PWRs). The cause of the accelerated corrosion has yet to be identified. This work identifies the potential for amorphous ZrO_2 phase stabilization by lithium that will potentially have an impact on the passive oxide's grain boundary structure. Higher lithium concentrations are found to stabilise the amorphous phase's stability before re-crystallisation to higher temperatures. Chemical assessment has also shown the lithium phase to be soluble in water, indicating a potential mechanism for lithium to alter grain boundaries and increase the pathways for further oxidation of the underlying zirconium material.

1. Introduction

Zirconium alloys are widely used in pressurised water reactors (PWRs) as a fuel cladding material due to their high corrosion resistance under normal operating conditions, and their low neutron cross section (Hallstadius et al., 2012). PWRs often adopt a coolant chemistry including boron to capture neutrons, in the form of H_3BO_3 acid, to provide a "shim" for reaction, reducing the overall reactivity of the core instead of relying on control rod movements, which requires a pH balance to reduce the corrosion by additions of lithium in the form of LiOH (Pastina et al., 1999). The pH is required to be elevated to between 7 and 7.4 to mitigate the corrosion of nickel-based alloys, water-wetted stainless steels and zirconium alloys (Song and Lee, 2003) (see Fig. 1).

The build-up of boron within the CRUD (Chalk River Unidentified Deposits) materials on the Axial offset anomaly periphery of the rod that forms in high burn-up regions within the reactor have been found to have a detrimental impact on reactor efficiency (Frattini et al., 2001; Blok et al., 2002). New proposals of small modular reactor (SMR) operation are considering a boron-free coolant design to limit the boron axial offset anomaly (Hulme et al., 2021; Mart et al., 2014; Sanchez and dos Santos, 2021). In the absence of boron, however, the phenomenon known as lithium accelerated corrosion of the zirconium-based alloy cladding has been widely reported (Hulme et al., 2021; Pêcheur et al., 2000, 2009; Murgatroyd and Winton, 1967; Ramasubramanian, 1991; Bramwell et al., 1991; Jeong et al., 1999; Motta et al., 2005; Ramasubramanian et al., 2008; Cox et al., 1998; Billot et al., 1993). To understand the mechanism of this accelerated corrosion, all aspects of the oxide that forms on the zirconium alloy require investigation to understand how Li could increase the availability of oxygen to the metal oxide interface. Literature suggests that the oxide formed at the metal oxide interface is tetragonal ZrO_2, which is stress stabilised (Liao et al., 2020; Qin et al., 2007), at the metal oxide interface that provides corrosion resistance. This gives way to a more relaxed monoclinic oxide further from the metal surface that offers little protection (Kurpaska et al., 2016; Eichler et al., 2004; Polatidis et al., 2012). Experimental work, however, has shown that the average phase fraction between monoclinic and tetragonal ZrO_2 shows no clear link between tetragonal layer thickness and corrosion resistance (Swan et al., 2016).

Previous atomistic simulation work had been conducted and found that the solution of Li into the bulk, tetragonal and monoclinic, ZrO_2 was expected to be extremely low (Stephens et al., 2021). Atom probe experiments have shown that Li levels in the matrix of oxides formed on Zircaloy-4 are close to the resolution limit, but Li segregates along the grain boundaries within the ZrO_2 oxide, lending credibility to the simulation work on low bulk Li solution viability (Stephens et al., 2021; Styman et al., 2022).

* Corresponding author. CSEE Dean Street, Bangor, LL57 1UT, Gwynedd, UK.
E-mail address: g.stephens@bangor.ac.uk (G.F. Stephens).

https://doi.org/10.1016/j.pnucene.2024.105165
Received 8 December 2023; Received in revised form 30 January 2024; Accepted 4 March 2024
Available online 12 March 2024

The complexity between grains has been shown to contain disordered amorphous structures where thermodynamically stable ZrO_2 can produce higher complexity structures (Cantwell et al., 2014). The work of (Styman et al., 2022) shows that some form of grain boundary complexity can be assured with a degree of amorphous structure uncertainty expected. Amorphous structures can be expected to form more readily at lower temperatures due to limited kinetic energy availability for crystalline atomic orientations (below 450 °C (Lebeau et al., 2020)). Further atomic scale simulation work has been undertaken to assess transport mechanisms of lanthanide dopants through the disordered oxide grain boundary (Owen et al., 2021) Recent atomistic modelling has identified an indication of Li solution in the amorphous structures coupled with an associated increase of vacant oxygen defects as a result (Stephens et al., 2023).

This investigation prepared and characterised amorphous oxides with different Li levels to support the simulations and provide extra insight into the behaviour of the surrogate grain boundary material. It also looked at the impact of Li stabilizing an amorphous structure, analogous to a highly complex grain boundary, which have been found through simulation to potentially modify grain boundary mobility of corrosive species (Owen et al., 2021; Stephens et al., 2023).

2. Method

The experimental stages began with the synthesis of lithium doped and undoped amorphous zirconia at low temperatures. These samples were then characterised to ensure there was no long-range order. Each sample was then thermally analysed up to 700 °C using simultaneous thermal analysis (DSC and TGA) to identify any transition temperatures. Post thermal treatment, further characterisation was conducted to analyse the product including the propensity for lithium to remain in the resulting structures.

2.1. Sample preparation

Samples of amorphous ZrO_2 were prepared, containing a wide range of Li concentrations (as shown in Table 1) to simulate the range that might be seen as the grain boundary compositions built up to the levels seen in atom probe analyses.

Amorphous ZrO_2 samples containing Li levels above 0.1 mol % were prepared by placing zirconium *n*-butoxide $Zr(OC_4H_9)_4$ solution (7 mL, 2.19 M, 80 wt% in n-butanol) in a round bottom flask (100 mL) and stirring in $LiOC(CH_3)_3$. Different amounts of $LiOC(CH_3)_3$ were added to produce solutions with a range of 0.1–60 mol % Li, as given in Table 1. The mixture was then stirred for 1 h at 70 °C under reflux. Deionised water (equivalents listed in Table 1) was added dropwise, and the resulting mixture was stirred under reflux at 70 °C for 2 h. The reflux apparatus was removed, and the solution was added to a flat bottom flask, and the mixture stirred overnight at 90 °C on a magnetic mixing hotplate until the solvent evaporated completely.

For lower concentrations of Li, a diluted solution was produced with $LiOC(CH_3)_3$ in n-butanol (12.5 mM, 100 mL) and was prepared using the following procedure: lithium *tert*-butoxide (0.1 g, 12.5 mmol) was weighed using an analytical balance within a glovebox at positive argon pressure. The solution was then poured into a volumetric flask (100 mL) and made up with n-butanol. This could then be transferred to the zirconium *n*-butoxide and butanol solution and placed under reflux prior to deionised water being added, as described above.

The water contents of the solutions used to produce oxides with higher Li contents were increased to ensure there would be sufficient water molecules to facilitate hydrolysis of both zirconium n-butoxide and Li t-butoxide.

The residues left after the solvent evaporated were approximately 2.5 ± 0.5 g, dependent on Li concentration, of very fine white powder.

2.2. Characterisation

The structure of the powder was analysed using Raman spectroscopy and X-ray diffraction (XRD) to ensure that the oxide was amorphous in the first instance and then again to ensure crystallisation had taken place post thermal analysis.

Raman spectroscopy was performed using the Bruker SENTERRA II using a 532 nm laser at 25 mW and a 15 μm aperture with a combination of 20 and 50 times optical lenses. The integration time was 1 s with a combined 5 coadditions with a 4 × 4 2D map of which an average was taken.

Bragg-Brentano reflection powder diffraction was performed with the Malvern Panalytical Aeris XRD with an Empyrean Cu LFF HR X-ray tube.

2.3. Thermal treatment and product characterisation

The crystallisation temperature of the amorphous structure was assessed whilst simultaneously conducting gravimetric analysis and mass spectroscopy using the Netzsch STA 449 F-series combined with the Netzsch QMS 403 Aëolos Quadro mass spectrometer. This permitted monitoring of the gases evolved during heating. A platinum crucible containing <1 g of the amorphous Li doped sample was heated with a ramp up rate of 15 °C/min up to 700 °C, held at 700 °C for 5 min, then cooled at 15 °C/min to 35 °C. Raman and XRD were subsequently conducted to confirm the final sample structure.

Transmission electron microscopy (TEM) was used to determine the location of the lithium in the dried powder. The TEM samples were prepared by placing a droplet of 50 mol % Li – ZrO_2 in suspension in deionised water onto a copper grating with carbon membrane. The grating was then left in a desiccator for sufficient time to let the solution dry out, leaving the ZrO_2 powders on the membrane. The sample was then put into a JEOL ARM 200F (S)TEM operating at 200 kV equipped with a Gatan GIF Quantum 965 ER, which was capable of Electron Energy Loss Spectroscopy (EELS) analysis. Spectral images containing several ZrO_2 powders were taken, with the spectra covering the Li K edge at an energy resolution of 0.25 eV/channel. The total acquisition time for each pixel was 0.1 s.

Inductively coupled plasma optical emission spectroscopy (ICP-OES) was used to analyse samples held in suspension to identify any lithium that may dissolved into the deionised water. For comparison, a known amount of solid sample was also digested in nitric acid and H_2O_2. The digested samples and suspension were filtered using 0.45 μm filters before ICP-OES analysis using an Agilent 5800 spectrometer. Samples were measured at the primary, secondary and tertiary emission wavelengths and their responses compared to those of lithium and zirconium ICP standards (from Sigma Aldrich).

3. Results

3.1. Synthesis of amorphous ZrO_2

The x-ray patterns from all of the powders yielded broad humps characteristic of amorphous/disordered material, while the Raman spectrum consisted of a broad tongue suggestive of a low symmetry/amorphous substance. The synthesis of lithium doped ZrO_2 was thus successful in producing amorphous ZrO_2 containing Li concentrations of 0, 5, 10, 20, 30, 40 and 50 mol %. XRD and Raman spectroscopy produced broad spectra, void of any long-range order and agrees well with previous results from both modelling and experiment (Rushton et al., 2019a). The region of interest for zirconia through Raman spectroscopy

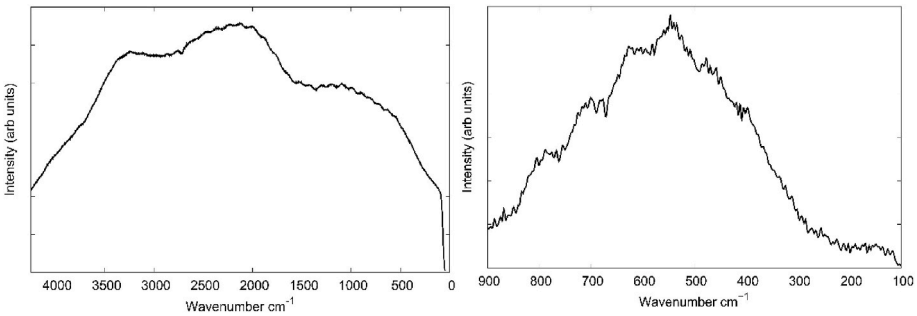

Fig. 1. Raman spectrum of (a) full wavenumber range and(b) focused between 100 and 900 $cm^{-1}$with a simple linear baseline correction. Both are typical of those taken from the synthesised compositions. Spectra quantify as the broad peaks/humps are indicative of amorphous ZrO_2.

Table 1
Li concentrations, required mass of Li tert-butoxide and deionised water volume used in final oxide of ZrO_2 synthesis.

Li concentration (mol %)	Li *tert*-butoxide mass (g)	Deionised water (mL)
0	–	1.13
0.1	0.0013	1.13
1	0.013	1.13
5	0.065	1.13
10	0.13	1.4
20	0.26	2
30	0.39	3
40	0.52	4
50	0.65	5
60	0.78	5

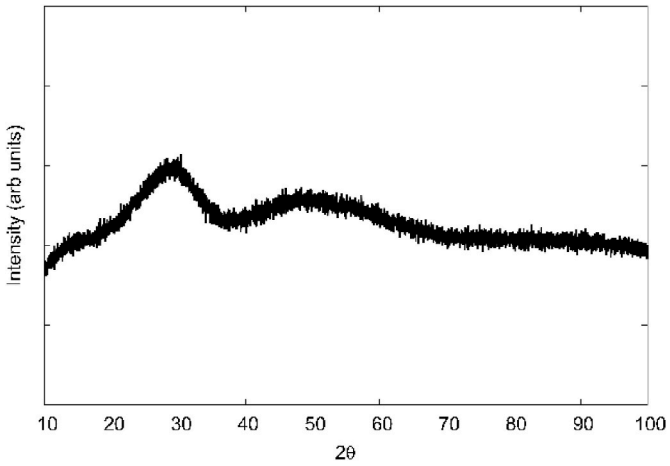

Fig. 2. XRD spectra typical of those taken from the synthesised compositions. Spectra quantify as the broad peaks/humps and are indicative of amorphous ZrO_2.

is found between 100 and 900 cm^{-1} in the literature (Ciszak et al., 2019).

3.2. Mass spectroscopy and thermogravimetric analysis

During thermal analysis, the mass change was monitored with the addition of mass spectroscopy to identify gas products produced from the sample during the heating, dwell, and cooldown process (see Fig. 2). Due to variations in sample dryness, and predictable thermogravimetric changes as a result, the sample mass reduction continued at a steady rate for all samples and reached equilibrium at around 450 °C. When viewing the results of mass spectroscopy data in real time, no real changes between samples could be identified where all samples produced H_2, H_2O, CO, O_2, and CO_2 when the argon environment data had been removed. But no Li, including molecular variants, were identified indicating that the Li was expected to have remained within the sample. To highlight this, the maximum ion current for all mass over charge numbers was taken for each sample throughout the heat, dwell, and cooldown processes (Fig. 3 a).

Each ion from the mass spectrometer could be related to temperature and time during the experiments. When considering H_2O water vapour produced from samples during the heating stage for 0 and 5 mol % Li ZrO_2 samples, these showed a sudden peak in water vapour production that also coincided with a change in morphology for the corresponding samples, which will be discussed later. These peaks are not evident for samples with a Li concentration of 10 mol % and above.

3.3. Simultaneous thermal analysis (STA)

Identifying the temperature associated with a change in morphology through simultaneous thermal analysis (STA) provides an indication of structure crystallisation from Li dopants. This is presented as a dip in DSC (Differential Scanning Calorimetry) which is representative of an increase of heat flow from the sample (Fig. 4 a) and an exothermic reaction. No meaningful results were obtained from smaller concentrations below 5 mol % Li which were similar to zero Li samples and were omitted.

The results reported in Fig. 4 show a clear relationship between lithium concentration and the stabilization of the initial amorphous structure. An exothermic peak was observed in each sample, highlighting a structural transformation, and this peak tends to broaden with increasing Li content. For the higher concentrations of Li considered (>10 mol %), a fairly linear relationship is observed, whereas the low concentration (0 and 5 mol %) do not follow this trend which would indicate a non-linear relationship.

3.4. Analysis of post STA samples using XRD and Raman spectroscopy

The post heat-treatment samples were subsequently analysed using XRD and Raman to assess the structures formed after the observed transformation from the amorphous structures (Fig. 4).

Whilst the Raman peaks gained were of low relative intensity, there were indications of both tetragonal and monoclinic structures when compared to the literature (Ciszak et al., 2019). The monoclinic doublet can be seen around the 200 cm^{-1} area with the tetragonal peak around 280 cm^{-1}. This may indicate that the local bonding is similar to that observed in crystalline systems as is expected from modelling results (Rushton et al., 2019b). When comparing the peaks gained in Fig. 5 to literature XRD peaks, tetragonal ZrO_2 was apparent for all samples. However, Li doped samples exhibited the two peaks expected above and below 30° 2θ which coincide with monoclinic ZrO_2. These peaks are small in comparison to the main 30° 2θ peaks so are not labelled in Fig. 5. Whilst small peak shifts were evident, there was no trend that could be associated with Li incorporation within the structure that could follow a change in Li concentration. Lithium compounds that were considered were $Li_{1.8}ZrO_3$, Li_2ZrO_3, $Li_4Zr_3O_8$ and $Li_6Zr_2O_7$, none of

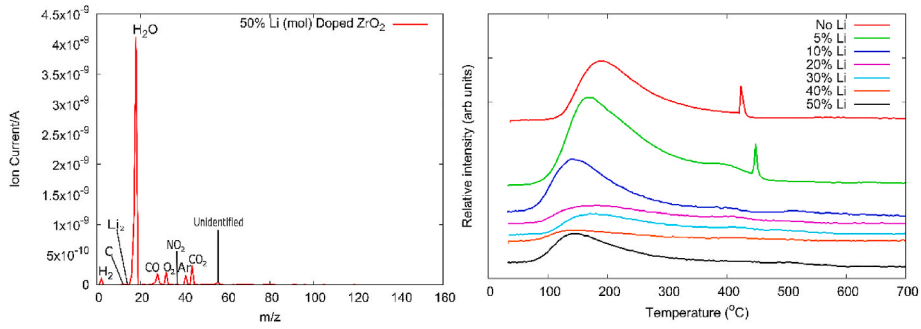

Fig. 3. a) Mass spectroscopy of maximum ion current through heat, dwell, cool down from 50 mol % Li in ZrO_2 b) Mass spectroscopy of water vapour from samples. The relative intensity of 0% and 5% Li peaks show an increase in water vapour produced between 400 and 500 °C.

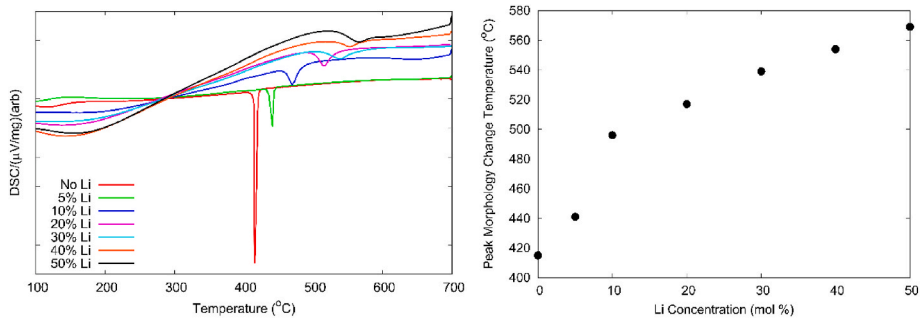

Fig. 4. Thermal analysis of samples where the reduction in differential scanning calorimetry (DSC) represents a sample morphology modification at a given temperature b) The Li concentration against the morphological modification temperature found as the peak value from figure a.

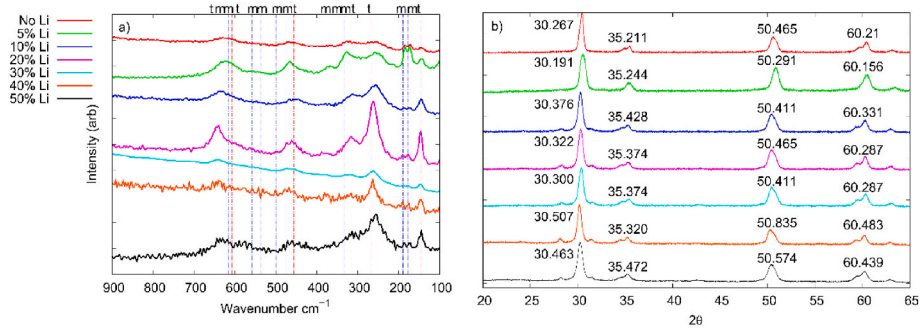

Fig. 5. A range of Li mol % concentrations in ZrO_2 for post STA samples in a) Raman spectroscopy with vertical dashed lines where red and labelled with a "t" is tetragonal and blue labelled with an "m" is monoclinic ZrO_2 and b) XRD.

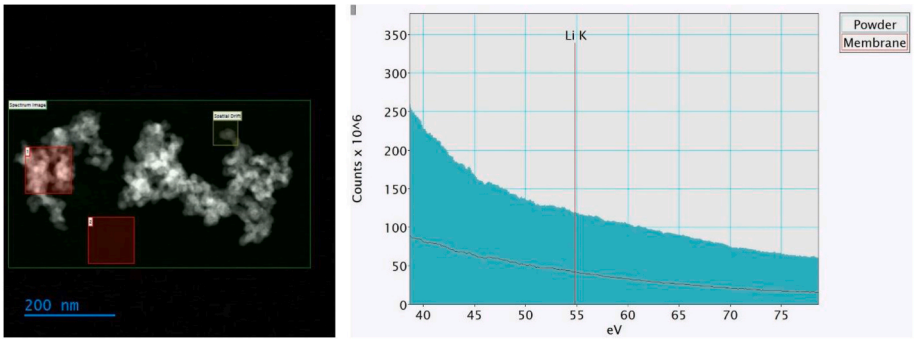

Fig. 6. Left, STEM HAADF image shows a cluster of ZrO_2 powder on a membrane. The green rectangle marks where the EELS mapping was undertaken. Red square 1 and 2 correspond to the two extracted spectra shown on right. No Li edge was identified in the spectra as the expected position is marked.

which were evident from the XRD analysis.

3.5. STEM with EELS

STEM with EELS were used to identify if Li had formed solution into the bulk ZrO_2. The structures were found to be between 10 and 20 nm in diameter and several electron energy loss spectral images were taken in the samples and no Li signal was detected in the ZrO_2 powders. An example is shown in Fig. 6.

As discussed in the method section, when preparing the samples for use in the STEM, they were placed in suspension in deionised water. This was then placed onto a copper grating with carbon membrane and allowed to dry. With the EELS results, this gave an indication that the lithium had been dissolved within the deionised water, leaving only the ZrO_2 crystals in suspension.

3.6. ICP-OES (Inductively coupled plasma optical emission spectroscopy)

As no Li containing phases were specifically identified in the XRD analysis or STEM with EELS, the location and form of the Li required further assessment.

The experiment was divided into two part assessing lithium in post heat treated 50% Li doped zirconia (up to 700 °C) with the first being conducted on the powder form (solid) and the latter being lithium doped zirconia that had formed suspension/solution in deionised water. For the solid sample, Li showed 3.63 mg/g with Zr showing 26.17 mg/g. However, the solution in the deionised water found Li at 1.51 mg/l and only 0.29 mg/l of Zr. This provides evidence that the lithium had formed a solution in the deionised water where the zirconia remained in suspension. The ratio of lithium to zirconium in the solid material was therefore 1.0/7.2 whilst in suspension it was 1.0/0.2. This shows in the digested solid there was a seven-fold higher level of zirconium than lithium present but in the solution, there was a fivefold higher level of lithium than zirconium present. This indicated that the lithium was solubilised within the water portion of the suspension. To confirm that no changes to the structure of ZrO_2 had taken place whilst held in suspension, all samples were later placed in deionised water, filtered, and then washed with further deionised water in filtration. The remaining ZrO_2 samples were analysed by XRD, confirming that no changes in structure, tetragonal and monoclinic ZrO_2, could be identified.

4. Discussion

This work primarily set out to identify how lithium would affect complex grain boundaries by creating a range of Li concentrations of doped amorphous ZrO_2 and finding if higher lithium concentrations would stabilise or destabilise the amorphous structure at the first instance of morphological change. The secondary goal, from this, was to verify if Li would or would not form a solution within bulk amorphous ZrO_2. Previous simulated work indicated that Li would have very limited solubility (Stephens et al., 2021). During STEM with EELS experiments, lithium was found to be absent within the samples which resulted in an additional investigation to identify the location of lithium.

In this work, the synthesis of amorphous ZrO_2 and 5, 10, 20, 30, 40 and 50 mol % Li doped amorphous ZrO_2 were successfully created and confirmed with both XRD and Raman spectroscopy through the characteristic absence of crystal peaks. The crystallisation of each sample was achieved noting the temperature at which this took place through STA and showed that higher Li concentrations required higher temperatures to form crystals. This provided evidence of the stabilization of the amorphous structure due to Li. The trend at which lithium stabilizes the amorphous $ZrO_2$is a little less clear. This could be interpreted in one of two ways. Above 5 mol %, the results could be considered as fairly linear but, when omitting 10 mol % Li, the results could be considered parabolic.

To ensure that no Li escaped the change in polymorph, during crystallisation, mass spectroscopy of the gases released from the samples were monitored and showed no indication of Li loss. In samples containing 5 mol % or less, water vapour was produced from the sample at the point of crystallisation but not at higher Li concentrations. This could be a result of Li forming an oxide/hydride or hydroxide which would lower the availability of H_2O to be released during the change in morphology from amorphous to tetragonal ZrO_2. This could also provide evidence to suggest that the STA crystallisation temperature vs lithium concentration at $\leq$5 mol % present a different reaction (water vapour release) and the trend is linear above these concentrations due to the formation of lithium hydroxides.

Post STA XRD analysis confirmed crystallisation of samples and that they were predominantly tetragonal, with a small increase of monoclinic ZrO_2 from samples containing more than 5 mol % Li. Previous work using a sol-gel route have shown that the change from the tetragonal to monoclinic polymorph is temperature dependant in pure ZrO_2 which should completely transform to monoclinic between 800 and 1000 °C (Aguilar et al., 2001). This would explain the introduction of the monoclinic phase into the samples when heated to 700 °C. Given that no monoclinic peaks were apparent in zero and 5 mol % Li here at the same temperatures, this would indicate that Li may be allowing stress relief within the material, such that a proportion of the tetragonal ZrO_2 is transforming to monoclinic ZrO_2 at lower temperatures. Whilst Li may stabilise the amorphous structures, it may also destabilise the tetragonal structures.

Grain size has also reportedly been between 5 and 27 nm in literature up to 800 °C (Aguilar et al., 2001). Raman spectroscopy showed limited results due to small crystal size that was later confirmed through STEM which showed crystal sizes to be between 10 and 20 nm. In addition to this, no evidence could be gained to indicate that Li formed solid solution in bulk ZrO_2 which confirmed previous simulation work that showed limited solubility (Stephens et al., 2023). Samples that were placed in deionised water resulted in the suspension of ZrO_2 and the dissolution of Li from the samples. This, too, was confirmed through STEM with EELS and, subsequently, ICP-OES which identified Li in solution within the deionised water. To ensure that no changes to ZrO_2 structure had taken place, samples were placed in deionised water, filtered and then rinsed through filtration with additional deionised water. These samples were then placed through XRD and provided no evidence of change from the bulk ZrO_2 samples.

Whilst this method does not consider any stress that may occur within grain boundaries themselves, the amorphous ZrO_2 provides a good surrogate to provide an indication of potential stabilization effects that Li may produce when incorporated into the grain boundaries.

Simulation work indicated that Li doped amorphous ZrO_2 may increase the vacant oxygen defects found within the grain boundaries (Stephens et al., 2023). When coupled with Li stabilization of the grain boundaries, this may provide a route to increase oxygen flux through the oxide and increase corrosion of the metal surface. It is possible that Li promotes grain boundary, amorphous, growth over bulk material. Furthermore, the amorphous phase may be able to accommodate lattice expansion and grain rotation, so, the early stress-stabilised tetragonal zirconia more quickly transforms to the monoclinic form. This might promote oxide grain nucleation over growth, so does not get the preferential columnar growth in the monoclinic oxide grains that are indicative of a more protective oxide in non-accelerated water-grown oxide films (Pècheur et al., 2000, 2009; Yankova et al., 2023). It is also possible that Li promotes grain boundaries that are undercoordinated in oxygen and allow a path for oxygen to “hop” to the metal surface (Owen et al., 2021). This indicates that a high oxygen vacancy concentration may produce a high oxygen flux through the grain boundaries. Whilst this work offers some answers, it also provides a focus for further questions such as the position or structure that Li might take (e.g., as a hydroxide) in-situ or in the post heat treated structures.

5. Conclusion

The result of this investigation indicate that lithium stabilizes the amorphous structure as the crystallisation temperature increased with increasing lithium concentration, producing a predominantly tetragonal polymorph. An increase in Li also promotes the monoclinic phase to form. During the formation of the bulk ZrO_2, the Li remains within the sample, but is not found within the crystals themselves, but outside of the crystals. It was found that the segregated Li after crystallisation was highly soluble in water. When combined with simulation work indicating that lithium can increase vacant oxygen concentrations and increase oxygen diffusion (Owen et al., 2021; Stephens et al., 2023), this experimental work provides additional potential to understand the accelerated corrosion of zirconium alloys in the presence of Li and opens a range of investigative avenues that may be explored. In-situ XPS may be used to identify the form lithium takes once segregated from grain boundaries during crystallisation. APT might be utilized to identify the depth of which lithium might reach into the oxide and/or if it is able to interact with the metal/oxide interface, which may affect grain and grain boundary growth (Li has been previously found at the M/O interface (Garner et al., 2023)). TKD could be used to identify the changes from columnar grain growth to equiaxial grains and, should lithium further promote grain boundary growth, smaller equiaxial grains.

CRediT authorship contribution statement

Gareth F. Stephens: Writing – original draft, Methodology, Investigation, Formal analysis, Conceptualization. **Jack A. Wilson:** Methodology, Investigation. **Simon F. Curling:** Writing – review & editing, Methodology, Investigation. **Guanze He:** Writing – review & editing, Methodology, Investigation. **P. John Thomas:** Writing – review & editing, Methodology. **David W. Williams:** Writing – review & editing, Methodology. **Susan Ortner:** Writing – review & editing, Supervision, Conceptualization. **Chris Grovenor:** Writing – review & editing, Supervision, Methodology. **Michael J.D. Rushton:** Writing – review & editing, Supervision. **Aidan Cole- Baker:** Writing – review & editing, Supervision, Funding acquisition. **Simon C. Middleburgh:** Writing – review & editing, Supervision, Project administration, Funding acquisition, Conceptualization.

Declaration of competing interest

The authors declare the following financial interests/personal relationships which may be considered as potential competing interests: Gareth F Stephens reports financial support was provided by Engineering and Physical Sciences Research Council. Nuclear Energy Futures Centre for Doctoral Training (EP/S023844/1). Gareth F Stephens reports financial support was provided by Jacobs UK Limited London.

Data availability

Data will be made available on request.

Acknowledgments

SCM, and MJDR are funded through the Sêr Cymru II programme by Welsh European Funding Office (WEFO) under the European Development Fund (ERDF). GFS is funded through the Nuclear Energy Futures Centre for Doctoral Training (EP/S023844/1), co-sponsored by Jacobs Engineering Group.

References

Aguilar, D.H., Torres-Gonzalez, L.C., Torres-Martinez, L.M., Lopez, T., Quintana, P., 2001. A study of the crystallization of ZrO_2 in the sol-gel system: ZrO_2-SiO_2. J. Solid State Chem. 158, 349–357. https://doi.org/10.1006/jssc.2001.9126.

Billot, P., Cox, B., Ishigure, K., Johnson Jr., A.B., Lemaignan, C., Nechaev, A.F., Petrik, N. G., Reznichenko, E.A., Ritchie, I.G., Sukhanov, G.I., 1993. Corrosion of Zirconium Alloys in Nuclear Power Plants. IAEA TECHDOC, p. 684.

Blok, J., Chauffiriat, S., Frattini, P., 2002. Modeling the axial offset anomaly in PWRs. In: Proceedings of International Conference on Water Chemistry of Nuclear Reactor Systems–Operation Optimisation and New Developments, pp. 1–9.

Bramwell, I.L., Parsons, P.D., Tice, D.R., 1991. Corrosion of Zircaloy-4 PWR Fuel Cladding in Lithiated and Borated Water Environments. http://inis.iaea.org/Search/search.aspx?orig_q=RN:23052627. (Accessed 2 May 2023).

Cantwell, P.R., Tang, M., Dillon, S.J., Luo, J., Rohrer, G.S., Harmer, M.P., 2014. Grain boundary complexions. Acta Mater. 62, 1–48. https://doi.org/10.1016/j.actamat.2013.07.037.

Ciszak, C., Mermoux, M., Gutierrez, G., Leprêtre, F., Duriez, C., Popa, I., Fayette, L., Chevalier, S., 2019. Raman spectra analysis of ZrO_2 thermally grown on Zircaloy substrates irradiated with heavy ion: effects of oxygen isotopic substitution. J. Raman Spectrosc. 50, 425–435. https://doi.org/10.1002/jrs.5513.

Cox, B., Kritsky, V.G., Lemaignan, C., Ritchie, I.G., Ruhmann, H., Shishov, V.N., Bibilashvili, YuK., Nikulina, A.V., Billot, P., Ishigure, K., Johnson Jr., A.B., Lemaignan, C., Nechaev, A.F., Petrik, N.G., Reznichenko, E.A., Ritchie, I.G., Sukhanov, G.I., 1998. Waterside Corrosion of Zirconium Alloys in Nuclear Power Plants. IAEA TECHDOC 996. https://www-pub.iaea.org/MTCD/Publications/PDF/te_996_web.pdf. (Accessed 24 May 2023).

Eichler, J., Eisele, U., Rödel, J., 2004. Mechanical properties of monoclinic zirconia. J. Am. Ceram. Soc. 87, 1401–1403. https://doi.org/10.1111/j.1151-2916.2004.tb07748.x.

Frattini, P.L., Blok, J., Chauffriat, S., Sawicki, J., Riddle, J., 2001. Axial offset anomaly: coupling PWR primary chemistry with core design. Nucl. Energy 40, 123–135.

Garner, A., Gillen, C., Stephens, G., Styman, P., Armson, S., Robinson, J., Liu, J., Carruthers, A., Pickering, F., Sherry, S., Chan, C., Fenwick, M., Hulme, H., Ortner, S., Riley, C., Grovenor, C., Frankel, P., Middleburgh, S.C., Cole-Baker, A., 2023. Understanding the Mechanistic Role of Lithium in Accelerated Corrosion of Zirconium Alloys Using Advanced Characterisation and Atomistic Simulation. ASTM, pp. 356–386. https://doi.org/10.1520/STP164520220054.

Hallstadius, L., Johnson, S., Lahoda, E., 2012. Cladding for high performance fuel. Prog. Nucl. Energy 57, 71–76. https://doi.org/10.1016/j.pnucene.2011.10.008.

Hulme, H., Panteli, A., Pickering, F., Gass, M., Cole-Baker, A., Binks, P., Fenwick, M., Waters, M., Smith, J., 2021. Investigating the corrosion behaviour of zircaloy-4 in LiOH under a thermal gradient and two-phase flow regime. In: Zirconium in the Nuclear Industry: 19th International Symposium, pp. 537–563. https://doi.org/10.1520/stp162220190008.

Jeong, Y.H., Kim, K.H., Baek, J.H., 1999. Cation incorporation into zirconium oxide in LiOH, NaOH, and KOH solutions. J. Nucl. Mater. 275, 221–224. https://doi.org/10.1016/S0022-3115(99)00148-8.

Kurpaska, L., Jozwik, I., Jagielski, J., 2016. Study of sub-oxide phases at the metal-oxide interface in oxidized pure zirconium and Zr-1.0% Nb alloy by using SEM/FIB/EBSD and EDS techniques. J. Nucl. Mater. 476, 56–62. https://doi.org/10.1016/j.jnucmat.2016.04.038.

Lebeau, B., Naboulsi, I., Michelin, L., Marichal, C., Rigolet, S., Carteret, C., Brunet, S., Bonne, M., Blin, J.L., 2020. Amorphous mesostructured zirconia with high (hydro) thermal stability. RSC Adv. 10, 26165–26176. https://doi.org/10.1039/d0ra04824k.

Liao, J., Xu, F., Peng, Q., Yang, Z., Li, Z., Qiu, S., 2020. Research on the existence and stability of interfacial tetragonal zirconia formed on zirconium alloys. J. Nucl. Mater. 528 https://doi.org/10.1016/J.JNUCMAT.2019.151846.

Mart, J., Klein, A., Soldatov, A., 2014. Feasibility study of a soluble boron-free small modular integral pressurized water reactor. Nucl. Technol. 188, 8–19. https://doi.org/10.13182/NT13-135.

Motta, A.T., Yilmazbayhan, A., Comstock, R.J., Partezana, J., Sabol, G.P., Lai, B., Cai, Z., 2005. Microstructure and growth mechanism of oxide layers formed on Zr alloys studied with micro-beam synchrotron radiation. J. ASTM Int. (JAI) 2. https://doi.org/10.1520/JAI12375.

Murgatroyd, B.A., Winton, J., 1967. Hydriding Zircaloy-2 in lithium hydroxide solutions. J. Nucl. Mater. 23, 249–256. https://doi.org/10.1016/0022-3115(67)90157-2.

Owen, M.W., Rushton, M.J.D., Evitts, L.J., Claisse, A., Puide, M., Lee, W.E., Middleburgh, S.C., 2021. Diffusion in doped and undoped amorphous zirconia. J. Nucl. Mater. 555, 153108 https://doi.org/10.1016/j.jnucmat.2021.153108.

Pastina, B., Isabey, J., Hickel, B., 1999. The influence of water chemistry on the radiolysis of the primary coolant water in pressurized water reactors. J. Nucl. Mater. 264, 309–318. https://doi.org/10.1016/S0022-3115(98)00494-2.

Pêcheur, D., Godlewski, J., Peybernès, J., Fayette, L., Noé, M., Frichet, A., Kerrec, O., 2000. Contribution to the Understanding of the Effect of the Water Chemistry on the Oxidation Kinetics of Zircaloy-4 Cladding. ASTM Special Technical Publication. https://doi.org/10.1520/stp14328s.

Pêcheur, D., Godlewski, J., Billot, P., Thomazet, J., 2009. Microstructure of oxide films formed during the waterside corrosion of the zircaloy-4 cladding in lithiated environment. In: Zirconium in the Nuclear Industry: Eleventh International Symposium. https://doi.org/10.1520/stp16169s.

Polatidis, E., Frankel, P., Wei, J., Klaus, M., Comstock, R.J., Ambard, A., Lyon, S., Cottis, R.A., Preuss, M., 2012. Residual stresses and tetragonal phase fraction characterisation of corrosion tested Zircaloy-4 using energy dispersive synchrotron X-ray diffraction. https://doi.org/10.1016/j.jnucmat.2012.07.025.

Qin, W., Nam, C., Li, H.L., Szpunar, J.A., 2007. Tetragonal phase stability in ZrO_2 film formed on zirconium alloys and its effects on corrosion resistance. Acta Mater. 55, 1695–1701. https://doi.org/10.1016/j.actamat.2006.10.030.

Ramasubramanian, N., 1991. Lithium Uptake and the Corrosion of Zirconium Alloys in Aqueous Lithium Hydroxide Solutions. ASTM Special Technical Publication, pp. 613–626. https://doi.org/10.1520/stp25531s. Publ by ASTM.

Ramasubramanian, N., Precoanin, N., Ling, V., 2008. Lithium uptake and the accelerated corrosion of zirconium alloys. In: Zirconium in the Nuclear Industry: Eighth International Symposium, vol. 187. https://doi.org/10.1520/stp18865s, 187–15.

Rushton, M.J.D., Ipatova, I., Evitts, L.J., Lee, W.E., Middleburgh, S.C., 2019a. Stoichiometry deviation in amorphous zirconium dioxide. RSC Adv. 9, 16320–16327. https://doi.org/10.1039/c9ra01865d.

Rushton, M.J.D., Ipatova, I., Evitts, L.J., Lee, W.E., Middleburgh, S.C., 2019b. Stoichiometry deviation in amorphous zirconium dioxide. RSC Adv. 9, 16320–16327. https://doi.org/10.1039/c9ra01865d.

Sanchez, P.P., dos Santos, A., 2021. Prediction of the power peaking factor in a boron-free small modular reactor based on a support vector regression model and control rod bank positions. Nucl. Sci. Eng. 195, 555–562. https://doi.org/10.1080/00295639.2020.1854541.

Song, M.C., Lee, K.J., 2003. The evaluation of radioactive corrosion product at PWR as change of primary coolant chemistry for long-term fuel cycle. Ann. Nucl. Energy 30, 1231–1246. https://doi.org/10.1016/S0306-4549(03)00054-9.

Stephens, G.F., Than, Y.R., Neilson, W., Evitts, L.J., Wenman, M.R., Murphy, S.T., Grimes, R.W., Cole-Baker, A., Ortner, S., Gotham, N., Rushton, M.J.D., Lee, W.E., Middleburgh, S.C., 2021. The accommodation of lithium in bulk ZrO_2. Solid State Ionics 373. https://doi.org/10.1016/j.ssi.2021.115813.

Stephens, G.F., Owen, M.W., Ghardi, E.M., Fraile, A., Ortner, S., Rushton, M.J.D., Lee, W. E., Cole-Baker, A., Middleburgh, S.C., 2023. Assessing Li accommodation at amorphous ZrO_2 grain boundaries. J. Nucl. Mater. 588 https://doi.org/10.1016/j.jnucmat.2023.154780.

Styman, P., Garner, A., Robinson, J., Cole-Baker, A., Ortner, S., 2022. Characterising the Effect of Li on Zircaloy Corrosion.

Swan, H., Blackmur, M.S., Hyde, J.M., Laferrere, A., Ortner, S.R., Styman, P.D., Staines, C., Gass, M., Hulme, H., Cole-Baker, A., Frankel, P., 2016. The measurement of stress and phase fraction distributions in pre and post-transition Zircaloy oxides using nano-beam synchrotron X-ray diffraction. J. Nucl. Mater. 479, 559–575. https://doi.org/10.1016/J.JNUCMAT.2016.07.024.

Yankova, M.S., Garner, A., Baxter, F., Armson, S., Race, C.P., Preuss, M., Frankel, P., 2023. Untangling competition between epitaxial strain and growth stress through examination of variations in local oxidation. Nat. Commun. 14 https://doi.org/10.1038/s41467-022-35706-3.